Eco-Coasting Controller Using Road Grade Preview: Evaluation and Online Implementation Based on Mixed Integer Model Predictive Control

Yongjun Yan, Nan Li, Jinlong Hong*, Bingzhao Gao, Jia Zhang, Hong Chen, Jing Sun, and Ziyou Song*

***Abstract*—Coasting is a common method used in eco-driving to reduce fuel consumption by utilizing kinetic energy. However, in order to avoid excessive computation induced by integer coasting maneuvers, the powertrain model used in eco-driving controllers that rely on look-ahead road information has been oversimplified. This oversimplification assumes that the engine goes to idle when coasting, which significantly limits the fuel-saving potential. To address this issue, we propose an eco-coasting strategy that calculates the optimal timing and duration of coasting maneuvers using road information preview. Different from the engine-idling method, two control-oriented coasting methods, fuel cut-off method and engine start/stop method are formulated for the model-based optimal control. To evaluate and choose the best coasting mechanism for eco-coasting strategy, dynamic programming (DP) is performed to provide the globally optimal performance (i.e., benchmark results) for evaluating the engine-idling method, fuel cut-off method, and engine start/stop method. Based on the offline simulation results, the engine start/stop method consistently outperforms the fuel cut-off method in terms of both fuel consumption and travel time. This is attributed to the engine start/stop method eliminating the engine drag torque during deceleration, despite the additional energy cost required for engine restart being taken into account in the modeling, thus providing a fair evaluation. Then, the online performance of the eco-coasting strategy with engine start/stop mechanism is evaluated using Mixed Integer Model Predictive Control (MIMPC). We propose a tailored mixed-integer programming algorithm to facilitate online implementation. Simulation results show that the proposed eco-coasting strategy achieves near-optimal performance compared to DP and outperforms the rule-based method.**

***Index Terms*—Eco-coasting strategy; Engine start/stop mechanism; Mixed-integer model predictive control.**

* Corresponding author: Ziyou Song, Jinlong Hong.

Y. Yan is with the State Key Laboratory of Automotive Simulation and Control, Jilin University, Changchun 130022, China and also with the Department of Mechanical and Automation Engineering, The Chinese University of Hong Kong, Shatin, Hong Kong. This work was done when he was a visiting Ph.D. student in the Department of Naval Architecture and Marine Engineering, University of Michigan, Ann Arbor, MI 48109 USA (e-mail: yanyongjun18@gmail.com).

N. Li is with the Department of Aerospace Engineering, Auburn University, AL, USA (e-mail: nanli@auburn.edu)).

J. Hong, and B. Gao are with the Clean Energy Automotive Engineering Center, Tongji University, Shanghai, 201804, China (e-mail: hongjl@tongji.edu.cn; gaobz@jlu.edu.cn).

J. Zhang is with the School of Automation, Beijing Institute of Technology, Beijing 100081, China (e-mail: zhangjia@bit.edu.cn).

H. Chen is with the College of Electronic and Information Engineering, Tongji University, Shanghai 201804, China (e-mail: chenhong2019@tongji.edu.cn).

J. Sun is with the Department of Naval Architecture and Marine Engineering, University of Michigan, Ann Arbor, MI 48109 USA (e-mail: jingsun@umich.edu).

Z. Song is with the Department of Mechanical Engineering, National University of Singapore, Singapore 117575, Singapore and also with the Department of Naval Architecture and Marine Engineering, University of Michigan, Ann Arbor, MI 48109 USA (e-mail: Ziyou@nus.edu.sg).

NOMENCLATURE

A	Frontal projected area of vehicle, $[m^2]$.
C	Vector of constraints, $[-]$.
C_d	Coefficient of drag, $[-]$.
d_{min}	Minimum off steps, $[-]$.
d	Engine start/stop signal, $[-]$.
F_t	Traction force, $[N]$.
F_r	Resistance force, $[N]$.
f_r	Coefficient of rolling resistance, $[-]$.
g	Gravitational constant, $[-]$.
I_{engine}	Engine inertia, $[kg\,m^2]$.
G_{f}	Gear ratio of final reduction drive, $[-]$.
G_g	Gear ratio of gearbox, $[-]$.
L	Lagrangian equation, $[-]$.
M_f	Fuel consumption model in the distance domain, $[-]$.
m_{eff}	Effective mass of the vehicle, $[kg]$.
$\dot{m}_f$	Instantaneous fuel consumption rate, $[g/s]$.
N_h	Prediction horizon, $[-]$.
r	Wheel radius, $[m]$.
s	Space coordinate, $[m]$.
$\dot{s}$	Slack variable, $[-]$.
T_b	Brake torque, $[Nm]$.
T_e	Engine torque, $[Nm]$.
$T_{\text{final,1}}$	Final driveshaft torque of engine-idling method, $[Nm]$.
$T_{\text{final,2}}$	Final driveshaft torque of fuel cut-off method, $[Nm]$.
$T_{\text{final,3}}$	Final driveshaft torque of engine start/stop method, $[Nm]$.
v	Vehicle longitudinal velocity, $[m/s]$.
$\bar{v}$	Partial velocity variation, $[m/s]$.
z	Fuel cut-off signal, $[-]$.
$\dot{z}$	Collected primal variables, $[-]$.
z_{current}	Optimal binary variables among the current horizon, $[-]$.
z_{history}	History binary variables, $[-]$.
$\alpha_{1\sim4}$	Coefficients of fuel consumption model, $[-]$.
β	Weight of weighted sum method, $[-]$.
ΔE_{engine}	Energy required for cranking the engine, $[J]$.
Δs	Discretization distance, $[-]$.

Δv	Velocity reduction, $[m/s]$.
δE_v	Partial inertia energy, $[J]$.
δ	Extended 0/1 variables, $[-]$.
ε	Tolerance constant, $[-]$.
η	Gearbox efficiency, $[-]$.
ν	Dual variable, $[-]$.
λ	Dual variable, $[-]$.
ϕ	Slope data, $[^\circ]$.
ρ	Air density, $[[kg/m^3]]$.
ω_e	Rotational velocity of the engine, $[rpm]$.
ω_w	Rotational velocity of wheel, $[rpm]$.

ACRONYMS

$BSFC$	Brake Specific Fuel Consumption.
$BBSQP$	Integrated branch-and-bound method and sequential quadratic programming.
DP	Dynamic Programming.
FCO	Fuel Cut-Off.
KKT	Karush–Kuhn–Tucker condition.
MPC	Model Predictive Control.
$MIMPC$	Mixed Integer Model Predictive Control.
$MINLP$	Mixed Integer Nonlinear Programming.
$MIOCP$	Mixed Integer Optimal Control Problems.
NLP	Nonlinear Programming.
QP	Quadratic Programming.
SQP	Sequential Quadratic Programming.
SUV	Sports Utility Vehicle.
TCU	Transmission Control Unit.

I. INTRODUCTION

FOR on-road vehicles, the key to further improving fuel economy through eco-driving is to comprehensively incorporate and fully integrate the powertrain system with the driving environment represented by traffic conditions and digital maps. In solving eco-driving problems, researchers have primarily focused on simplifying and fitting fuel consumption maps with a single nonlinear convex function to optimize the engine work area with acceptable computational complexity [1], [2]. However, it is important to note that the fitted function may not be able to capture all engine conditions, as the trade-off between model complexity and fitting accuracy may result in the neglect of some fuel-efficient powertrain maneuvers during coasting, as discussed in prior research [3]. In reality, for a conventional car with a gasoline engine and automatic transmission, there are three methods to coast during the deceleration phase: setting the gear to neutral and turning off the engine [4], [5]; shutting off fuel injection when no torque is requested [6]–[8]; and manipulating the lock-up clutch to disconnect the engine from the powertrain when the engine is off [9]–[13].

Eco-coasting, as a category of eco-driving, refers to the strategies used to roll the vehicle with kinetic energy without traction force [14]. Most studies on eco-coasting have focused on evaluating the fuel economy benefit of different coasting strategies using backward vehicle simulation approaches [4], [15], [16]. In these simulations, the required engine load is calculated from the pre-defined vehicle speed profile, but this approach does not fully explore the potential of eco-coasting since the generated coasting action only relies on the current vehicle state and road information. Previous investigations have shown that look-ahead control can achieve better performance when the slope information on the road ahead is available [17]–[19]. To the best of the authors' knowledge, no research has been reported on the comparison of the fuel-saving potential among different coasting methods under cruising conditions with road grade preview, let alone the online implementation of these coasting strategies.

In the context of eco-coasting, Model Predictive Control (MPC) is a promising approach to calculate the timing and duration of coasting maneuvers, taking into account real-time execution capabilities and look-ahead road grade variations. However, the integer nature of engine start/stop and fuel cut-off coasting methods results in mixed-integer optimal control problems (MIOCPs), similar to those encountered in gear shift optimization [20], [21] and engine start/stop of hybrid vehicles [20], [22] in the field of online energy management. There are two open problems for the online implementation of eco-coasting strategies with an MPC controller: (1) frequent switching of integer coasting variables; and (2) computational burden. To reduce the switching frequency, researchers have proposed adding a penalty for switching frequency [20] or imposing inequality constraints that limit the total number of switch occurrences for integer variables [23]. These formulations can reduce switching frequency for a finite horizon open-loop optimal control problem. However, neither method is effective for MPC if the first element of the control sequence changes at different sampling instants due to numerical sensitivity to driving conditions. In [24], [25], mixed-integer linear inequalities are used in the MPC formulation to model the minimum amount of time that an on/off control variable must be kept on/off.

In terms of computational complexity, two general approaches exist for solving mixed-integer nonlinear programming (MINLP) problems: the first one involves solving the MINLP directly using the branch and bound method or related solvers, which can be computationally expensive [26]. The second approach is a heuristic method that relaxes the integer variables to continuous ones and reformulates the original MINLP into a non-linear programming problem (NLP), rounding feasible solutions to the nearest integer. Although this relax-and-round method is computationally efficient, it cannot guarantee optimality of the final solution [27], [28]. Richards $et\ al.$ have suggested that the MINLP for online control should be simplified by using knowledge of the control problem[29]. To this end, a warm-starting strategy has been proposed for the branch-and-bound algorithm that exploits the sequential nature of the problem to propagate information from previous branch-and-bound trees [30]. Early branching is another problem-specific technique used for fast solutions. In [31], an early branching rule is performed right after a single Quadratic Programming (QP) iteration of the Sequential Quadratic Programming (SQP) solver to detect infeasibility of the QP problem.

In this article, we propose a fuel-optimal eco-coasting controller for the eco-coasting problem by considering look-ahead road grade information from digital maps. We formulate two coasting frameworks, fuel cut-off, and engine start/stop,

in addition to the engine-idling powertrain model commonly used for eco-driving research, considering the engine drag torque and extra cost to restart the engine. By analyzing the results with the globally optimal one (i.e., benchmark result) derived by the dynamic programming, we choose engine start/stop as the best coasting mechanism due to the significant performance advantage with respect to a criterion that weighs trip time and fuel consumption. But given the DP solution's computationally prohibitive nature and inability to handle uncertainty and model mismatch in real-world applications, the eco-coasting control problem is reformulated following an MPC scheme that explicitly incorporates the vehicle coasting dynamics, road information, and cruise speed tracking performance into the energy minimization. Then, a holistic framework integrating the branch-and-bound and SQP algorithms is proposed for real-time implementation. Finally, a comprehensive comparison is conducted to assess the proposed MPC-based method, dynamic programming, and a rule-based controller. Simulation results show that the proposed eco-coasting method using road information preview can achieve significant fuel consumption reduction without compromising the travel time, close to the globally optimal solution. The novelties of this paper are summarized below:

1) We analyze the fuel optimal performance of three coasting frameworks (engine-idling, fuel cut-off, and engine start/stop) for the cruise control system under various road conditions to determine the best coasting method.

2) We develop a novel MPC-based eco-coasting controller with inequality constraints applied to the integer coasting variable to handle the frequent switch of the engine start/stop behaviors.

3) We demonstrate the fuel-saving performance and real-time capability of the proposed eco-coasting controller using the tailored mixed-integer programming algorithm.

The remainder of this paper is organized as follows: Section II provides background information on different vehicle coasting models; Section III presents the offline evaluation of the proposed coasting strategies; Section IV details the online implementation of the proposed eco-coasting methods with MPC scheme and the tailored mixed-integer programming algorithm; Section V discusses performance evaluation results and insights based on the simulation. Finally, conclusions and future work are concluded in Section VI.

II. Background and Different Vehicle Coasting Models

In this section, we begin by presenting the model of the test-bed vehicle, as well as the different coasting methods and formulations for calculating fuel consumption. For the purposes of this study, we utilize a conventional sports utility vehicle (SUV) that is powered by a combustion engine and a 6-speed automatic transmission, which allows us to demonstrate the specific design requirements of an eco-coasting controller under highway conditions. The proposed eco-coasting strategy can be integrated with the predictive cruise control system that was previously developed in our work [32]. As depicted in Fig. 1, the eco-coasting function is activated based on feedback from the vehicle's sensors and state.

A. Vehicle Model

Consider the longitudinal vehicle model described as

$$\begin{aligned} \dot{s} &= v, \\ \dot{v} &= \frac{1}{m_{\text{eff}}}\left[F_t - F_r(s,v)\right], \end{aligned} \tag{1}$$

where s is the distance traveled and v is the velocity, $\dot{s}$ and $\dot{v}$ are the derivative with respect to time t, m_{eff} is the total mass of the vehicle, F_t is the traction force and F_r is the total resistance force.

Table 1
Parameters of Vehicle

Symbol	Description	Value
m_{eff}	Effective mass of the vehicle	1870 kg
C_d	Coefficient of drag	0.373
A	Frontal projected area of vehicle	2.58 m^2
ρ	Air density	1.205 kg/m^3
f_r	Rolling resistance coefficient	0.011
g	Gravitational constant	9.8 m/s^2
η	Gearbox efficiency	0.94
r_w	Wheel radius	0.364 m
G_g	Gear ratio of gearbox	0.672
G_{f}	Final driver ratio	4.103
T_{drag}	Engine drag torque	30 N·m
I_{engine}	Engine inertia	0.15 $\text{kg}\cdot\text{m}^2$
α_1	Coefficient	0.2159
α_2	Coefficient	0.005676
α_3	Coefficient	0.0004349
α_4	Coefficient	8.899E-07

The total resistance force, F_r, consists of the aerodynamic resistance, the grade resistance, and the rolling resistance, as calculated by

$$F_r(s,v) = m_{\text{eff}} g\left(\sin(\phi(s)) + f_r\cos(\phi(s))\right) + \frac{C_d \rho A}{2} v^2, \tag{2}$$

where g is the gravitational constant, $\phi(s)$ is the slope data in the distance domain, f_r is the coefficient of rolling resistance, C_d is the drag coefficient, ρ is the air density, and A is the frontal projected area of the vehicle.

Assuming no slip on the wheel, the wheel rotational speed ω_w and traction force F_t can be calculated as:

$$\begin{aligned} \omega_w &= \frac{v}{r_w}, \\ F_t &= \frac{1}{r_w} T_{\text{final}}, \end{aligned} \tag{3}$$

where $T_{\text{final}} \in \{T_{\text{final},1}, T_{\text{final},2}, T_{\text{final},3}\}$ is the final driveshaft torque for engine-idling, fuel cut-off, and engine start/stop methods respectively, and r_w is the wheel radius.

The vehicle dynamic equations in (2) are defined in the time coordination. However, the slope information represented in the digital map is location-specific and is more naturally correlated to spatial information. To that end, we adopt the spatial-based model, as shown below

$$\frac{\mathrm{d}v}{\mathrm{d}t} = \frac{\mathrm{d}v}{\mathrm{d}s}\frac{\mathrm{d}s}{dt} = \frac{\mathrm{d}v}{\mathrm{d}s} v. \tag{4}$$

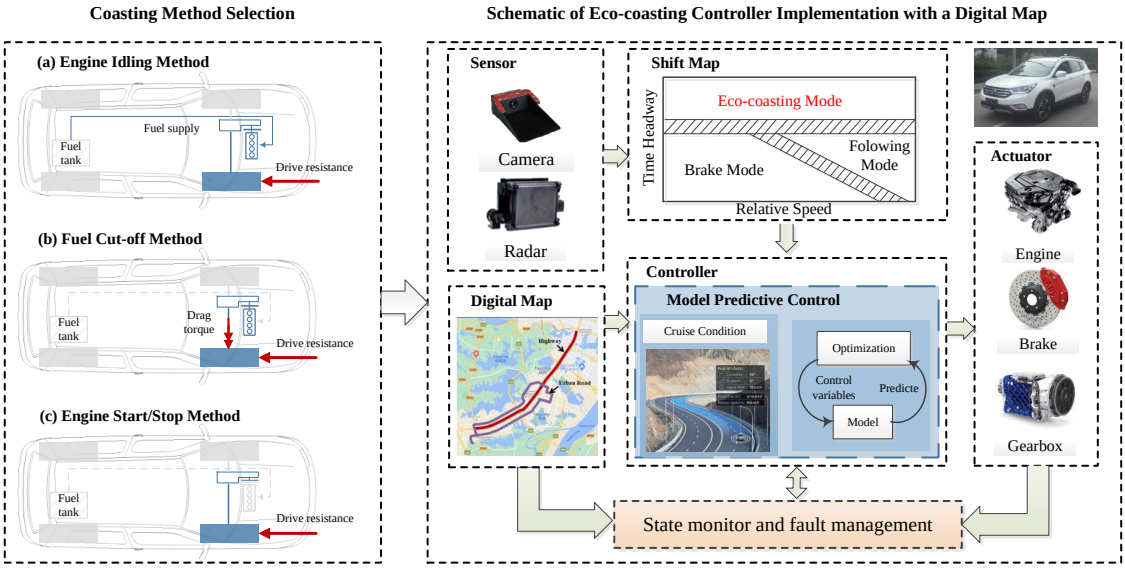

Figure 1. Illustration of different coasting methods and eco-coasting implementation with a digital map

The model in the spatial domain can be given as

$$\frac{\mathrm{d}v}{\mathrm{d}s} = \frac{1}{m_{\text{eff}}v}\left[F_t - F_r(s,v)\right]. \tag{5}$$

By applying Euler forward method and sampling in the s-domain, the vehicle dynamic model is discretized as

$$\begin{aligned} v(k+1) &= g\left(v(k), T_e(k), T_b(k)\right) \\ &= v(k) + \frac{1}{m_{\text{eff}}v(k)}\left[F_t - F_r(k\Delta s, v(k))\right]\Delta s, \end{aligned} \tag{6}$$

where Δs is the discretization distance in each step.

B. Different Coasting Methods

To quantify fuel consumption, a polynomial fuel consumption model is fitted using measurements obtained from the manufacturer's engine dynamometer. In-field tests are also conducted to measure the idle fuel mass flow rate, which is not included in the dynamometer measurements. The computational complexity and fuel cut-off mechanism are taken into consideration when constructing the following model:

$$\dot{m}_f = \alpha_1 + \alpha_2\omega_e T_e + \alpha_3\omega_e^2 T_e + \alpha_4\omega_e T_e^2, \tag{7}$$

where $\dot{m}_f$ $[g/s]$ is the instantaneous fuel consumption rate, and $\alpha_{1\sim4}$ are the constant coefficients as shown in Table 1. The comparison between the real and modeled maps of Brake Specific Fuel Consumption (BSFC) for the polynomial fuel consumption model is shown in Fig. 2. The BSFC map was measured by the engine manufacturers and provided by the OEM with whom we collaborated.

Note that:

- The polynomial equation includes a constant term to represent the idle fuel consumption;
- To avoid over-fitting and reduce computation burden, a 3rd-order polynomial is used;
- Engine torque affects every term in the equation, except for the constant one.

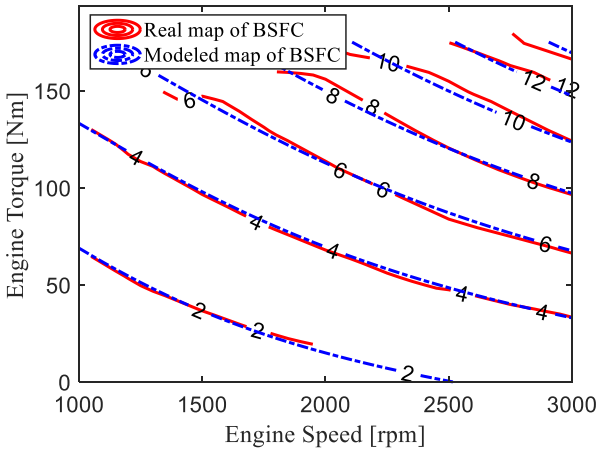

Figure 2. Comparison of the real (solid red) and modeled (dashed blue) BSFC [g/s] for the fitted polynomial fuel consumption model.

The reformulated fuel consumption in the distance domain is represented as

$$M_f(k) = \frac{\dot{m}_f\left(T_e(k)\right)}{v(k)}, \tag{8}$$

where $M_f(k)$ is the fuel consumption over the discretization step.

As shown in Fig. 1, three different coasting methods are considered and compared in this study.

1) Engine-idling Method: The high-efficiency area in the BSFC map corresponds to the highest gear setting of the transmission when the vehicle is cruising on the highway. The lock-up clutch remains engaged during this operation. Thus, taking into account the underlying physics and empirical knowledge, we formulate the control-oriented powertrain model

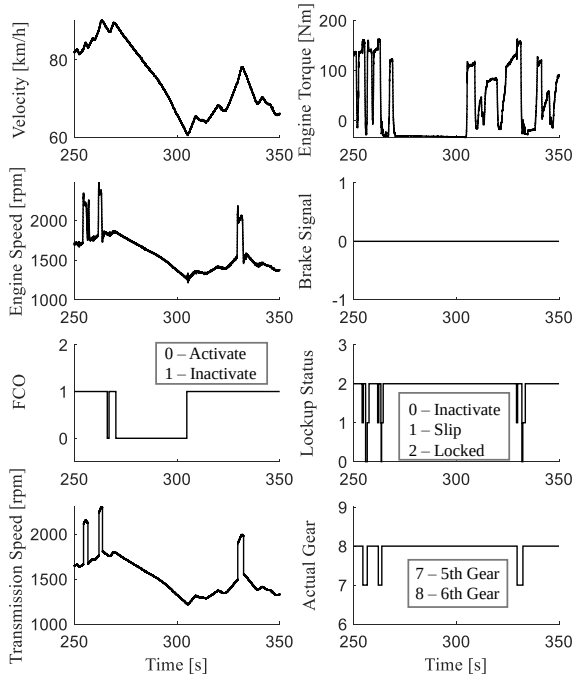

Figure 3. Field test data in Wuhan, China, with post-processed FCO signal. The FCO signal is represented by 0 when activated, and 1 when inactive, to facilitate the optimal control problem formulation.

as follows:

$$\begin{aligned} T_{\text{final},1}(k) &= \eta G_g G_{\text{f}} T_e(k) - T_b(k), \\ \omega_w(k) &= \frac{\omega_e(k)}{G_g G_{\text{f}}}, \end{aligned} \tag{9}$$

The torque of the final driveshaft, engine, and brake are denoted as T_{final}, T_e, and T_b, respectively, while ω_e represents the rotational velocity of the engine, η represents the transmission efficiency, and G_g and G_{f} are the gear ratios of the gearbox and final driveshaft, respectively. The engine torque, which is the "flywheel torque" of the engine, is obtained through the vehicle Controller Area Network (CAN). It is worth noting that the fuel consumption model (7) accounts for engine idling fuel consumption when the engine goes idle.

2) Fuel Cut-Off Method: The application of the fuel cut-off (FCO) strategy in engines has proven to be an efficient way to reduce fuel consumption. Fig. 3 displays the vehicle driving data collected on a test platform, where FCO is activated when the requested engine torque is zero. During FCO, the transmission is held in the highest gear by engaging the clutch while coasting. The negative engine torque observed in Fig. 3, as measured based on the experimental data, signifies the engine drag torque, which results from the resistance caused by pumping/throttling losses during fuel cut-off.

Based on the analysis of the field test data, the coasting dynamics with the FCO method can be discretized as

$$T_{\text{final},2}(k) = \eta G_g G_{\text{f}} \left(T_e(k) - (1-z) T_{\text{drag}}\right) - T_b(k), \tag{10}$$

where $z \in \{0, 1\}$ is the FCO signal representing the activation and inactivation of fuel cut-off, respectively. When the FCO is activated, the engine drag torque T_{drag} is constant, as shown in Fig.3. The fuel consumption model is modified as follows:

$$M_f(k) = \begin{cases} \frac{\dot{m}_f(T_e(k))}{v(k)} \Delta s, & z(k) = 1 \quad \text{(fuel injected)}, \\ 0, & z(k) = 0 \quad \text{(fuel off)}. \end{cases} \tag{11}$$

(11) reflects that there is no idle fuel consumption when fuel is cut off.

3) Engine Start/Stop Method: For a conventional vehicle, another fuel-efficient strategy during coasting is to turn off the engine and disengage the clutch. Then, the engine will be restarted by leveraging the slipping of the clutch powered by vehicle inertia. This clutch start method is superior to belt-driven starter systems or electric motors mounted on the engine's crankshaft in the high-speed cruising condition [16]. For simplicity, "Engine Start/Stop" refers to "Engine Start/Stop coordinated with the engagement or disengagement of the clutch". The powertrain model with engine start/stop mechanism is formulated as

$$T_{\text{final},3}(k) = \eta G_g G_{\text{f}} T_e(k) - T_b(k), \tag{12}$$

where the engine drag torque is eliminated thanks to the disengaged clutch.

After turning off the engine and disengaging the clutch, the engine's rotational speed decreases to zero, while the transmission's rotational speed becomes proportional to the vehicle speed due to the mechanical connection. To ensure a smooth re-engagement process, the transmission is kept in the highest gear, minimizing the speed difference of the clutch. High-speed cruise conditions typically require the highest gear for an efficient operation area of the engine, validating the assumption of a constant gear during this process. This assumption is supported by the experimental data in Fig. 3.

This restart process can be regarded as using the vehicle's kinetic energy to "recharge" the engine. The additional cost incurred to restart the engine is modeled based on the energy balance

$$\begin{aligned} \Delta E_{\text{engine}} &= \frac{1}{2} I_{\text{engine}} \left(\omega_e^2(k) - 0\right) \\ \omega_e(k) &= \frac{G_g G_{\text{f}} v(k)}{2\pi r_w}, \end{aligned} \tag{13}$$

where ΔE_{engine} represents the energy required for cranking the engine from rest to the synchronization speed of transmission. The engine's inertia is denoted as I_{engine}, and $\omega_e(k)$ is the engine speed after synchronization, which is proportional to the vehicle speed due to the engaged lock-up clutch. We assume that the engine start/stop and clutch engage/disengage process can be completed within one sampling interval in this study. When the engine is turned on at the kth step, the partial inertia energy of the vehicle will be transformed into engine inertial energy based on the energy balance. This transformation is formulated as

$$\frac{1}{2} m_{\text{eff}} v^2(k+1) = \frac{1}{2} m_{\text{eff}} v^2(k) + \left[F_t - F_r\right] \Delta s + \delta E_v(k), \tag{14}$$

$$\Delta E_{\text{engine}}(k) = \delta E_v(k) = \frac{1}{2} m_{\text{eff}} \left(\bar{v}^2(k+1) - v^2(k)\right). \tag{15}$$

Here, the partial inertia energy of the vehicle is denoted by δE_v, and $\bar{v}(k+1)$ is the corresponding partial velocity variation

caused by the engine start process within the current sampling interval. Thus, the velocity reduction caused by the engine start is formulated as

$$\Delta v(k) = \begin{cases} \bar{v}(k+1) - v(k) & \text{if } d(k) = 1 \text{ and } d(k-1) = 0 \\ 0 & \text{else .} \end{cases} \tag{16}$$

where $d \in \{0, 1\}$ is the engine start/stop signal, with 0 and 1 representing that the engine is turned off and turned on respectively.

The coasting dynamic with the engine start mechanism in the distance domain after the discretization can be expressed as

$$\begin{aligned} v(k+1) &= g\left(v(k), T_e(k), T_b(k)\right) \\ &= v(k) + \frac{1}{m_{\text{eff}} v(k)} \left[F_t - F_r\right] \Delta s - \Delta v(k). \end{aligned} \tag{17}$$

III. Evaluation of various eco-coasting methods

The main objective of the offline evaluation is to select the optimal coasting method, which will form the foundation for developing the MPC-based eco-coasting controller. This section summarizes the optimization problems related to the three coasting methods, and their performance is evaluated using DP under various slope profiles extracted from the digital map. The DP solution serves as the benchmark to evaluate the proposed controller in the next section. Additionally, we analyze the features of the optimal coasting maneuver when optimizing with look-ahead information to aid in the development of the subsequent controller.

A. Engine-idling Method

Given a predefined slope profile with a length of N, an optimization problem is formulated to find an optimal control law over the entire driving cycle. To balance fuel economy and trip time, both metrics are used in the cost function, and a weighted sum approach is employed to consider these conflicting objectives simultaneously. Therefore, the control problem can be formulated as:

$$\min_{T_e(.), T_b(.)} \sum_{i=0}^{N} (\beta(M_f(k)) + (1-\beta)\frac{1}{v(k)})\Delta s, \tag{18}$$

subject to the system dynamic constraints (6), (9) and

$$\begin{aligned} &0 \le T_e(k) \le T_{e,\max}, \quad k = 0 : N-1 \\ &0 \le T_b(k) \le T_{b,\max}, \quad k = 0 : N-1 \\ &v_{\min} \le v(k) \le v_{\max}, \quad k = 0 : N \\ &v(0) = v_0, v(N) = v_0, \end{aligned} \tag{19}$$

where $T_{e,\max}$ and $T_{b,\max}$ represent the maximum engine and brake torque constraints respectively, and $v_{\min}$ and $v_{\max}$ denote the lower and upper speed limits of the cruise range. The weight β balances the two conflicting objectives of fuel economy and trip time, and ranges between 0 and 1. In the engine-idling method, the vehicle speed $v(k)$ is the only state variable, while the engine torque T_e and brake torque T_b are the control variables. Given the prior information on the global road grade, the optimization problem aims to determine the control inputs $u(k) = [T_e(k), T_b(k)]$ that minimize the overall cost function subject to the state constraints and vehicle operating constraints. The initial and final speeds are fixed as v_0 to ensure a fair comparison.

B. FCO Method

In comparison to the engine-idling method, the optimal control problem for the fuel-efficient FCO method includes an integer control variable, fuel cut-off maneuver. To balance driving comfort with fuel efficiency, an additional penalty term is introduced in the cost function to limit the frequency of FCO signal switching

$$\begin{aligned} \min_{T_e(\cdot), T_b(\cdot), z(\cdot)} \sum_{i=0}^{N} (&\beta M_f(k) + (1-\beta)\frac{1}{v(k)} \\ &+ \alpha(z(k+1) - z(k))^2)\Delta s, \end{aligned} \tag{20}$$

where the additional term $(z(k+1) - z(k))^2$ penalizes the switching frequency of the FCO signal throughout the entire trip. To control the frequency, a weight coefficient α is used. The cost of (20) subject to the system dynamics (6), (10) as well as the constraints specified as follow:

$$\begin{aligned} &0 \le T_e(k) \le T_{e,\max} \cdot z(k), \quad k = 0 : N-1 \\ &0 \le T_b(k) \le T_{b,\max} \cdot (1 - z(k)), \quad k = 0 : N-1 \\ &v_{\min} \le v(k) \le v_{\max}, \quad k = 0 : N \\ &v(0) = v_0, v(N) = v_0 \\ &z(k) \in \{0, 1\}, \quad k = 0 : N-1. \end{aligned} \tag{21}$$

The constraints above ensure that $T_e(k) = 0$ when FCO is activated, and $T_b(k) = 0$ when FCO is inactivated. This condition automatically ensures that T_e and T_b will not be non-zero simultaneously. In the eco-coasting optimization problem, the vehicle speed $v(k)$ is the only state, while the engine torque T_e, brake torque T_b, and fuel cut-off signal $z(k)$ are considered as control variables.

C. Engine Start/Stop Method

Since the cost of engine restart is already incorporated in the dynamic equations (12) and (17), the penalty term $(d(k+1) - d(k))^2$ intended to limit frequent switching is unnecessary. Therefore, the cost function for engine start/stop control consists only of fuel consumption and trip time, and can be expressed as:

$$\min_{T_e(\cdot), T_b(\cdot), d(\cdot)} \sum_{i=0}^{N} (\beta M_f(k) + (1-\beta)\frac{1}{v(k)})\Delta s, \tag{22}$$

and the optimal solution should be subject to the vehicle dynamics

$$\begin{aligned} v(k+1) &= g\left(v(k), T_e(k), T_b(k)\right) \\ &= v(k) + \frac{1}{m_{\text{eff}} v(k)} \left[F_t - F_r\right] \Delta s - \Delta v(k). \end{aligned} \tag{23}$$

where the $\Delta v(k)$ is the velocity reduction caused by the engine start

$$\Delta v(k) = \begin{cases} \bar{v}(k+1) - v(k) & \text{if } d(k) = 1 \text{ and } d(k-1) = 0 \\ 0 & \text{else .} \end{cases} \tag{24}$$

The optimization problem formulation for the engine start/stop method is subject to the same state and control variable constraints as the fuel cut-off method described in (21), with the exception that the fuel cut-off signal $z(k)$ is replaced by the engine start/stop signal $d(k)$.

D. Dynamic Programming

To prove the eco-coasting strategy leveraging the engine start/stop mechanism outperforms the other two strategies, Dynamic Programming [17], as a global optimization approach, is used to derive the timing and duration of the coasting signal along with the engine torque and brake torque.

In this section, the optimal control problem is formulated in terms of the distance domain, and a distance grid is used in discrete DP. However, the distance s is not explicitly used as a state variable. Instead, the velocity v is discretized by Δv, and it is the only state variable in the optimal control problem (OCP). The search space is thus composed of the distance grid and the velocity grid. Backward iteration is used to solve the optimal control law by minimizing the cost-to-go function, which represents the cost required to reach the terminal set speed at the destination. The integer control variable representing the fuel cut-off signal is integrated into the backward iteration process naturally. Based on the field test data shown in Fig. 3, the required engine torque is zero when the fuel cut-off is activated. Therefore, the fuel cut-off is activated only if the calculated engine torque is zero during the velocity transitions from one stage to another.

The chosen grid size affects computational complexity and accuracy. Here, a 5m distance grid and a 0.1m/s velocity grid are used, along with other constraint parameters listed in Table 2. The maximum brake torque is set to 500 Nm to prevent sudden braking. The study evaluates the performance of different coasting strategies using DP on three slope profiles, including urban expressway sections in Chongqing and Wuhan, China (Fig. 4), and a typical uphill-downhill segment (Fig. 5).

Table 2
PARAMETERS OF OPTIMIZATION PROBLEM

Parameter	Description	Value
$v_{\min}$	Minimum of velocity	50/3.6 m/s
$v_{\max}$	Maximum of velocity	90/3.6 m/s
$T_{e,\max}$	Maximum of engine torque	120 N·m
$T_{b,\max}$	Maximum of brake torque	500 N·m
v_0	Initial and terminal velocity	75/3.6 m/s

E. Analysis of the Dynamic Programming Solution

Analyzing the characteristics of the globally optimized coasting maneuver obtained from the DP solution guides the subsequent controller development. Varying the weighting factor β allows for different relative emphases on each

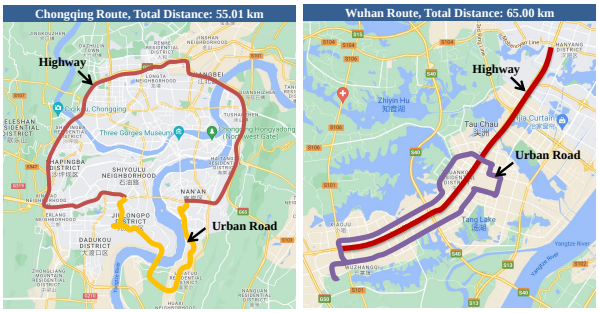

Figure 4. Route in Chongqing and Wuhan, China.

attribute to investigate performance trade-offs. The Pareto fronts provide insights into the trade-off between trip time and fuel consumption for different coasting methods, allowing the following remarks to be made.

Remark 1 (Coasting mechanisms): Fig. 5 shows that the engine start/stop strategy outperforms other strategies, as the vehicle turns off the engine in advance when approaching the destination and considering the terminal speed constraints (Fig. 6). The disengagement of the lock-up clutch during the engine-off period eliminates engine drag torque, leading to a moderate deceleration and longer coasting distance. Compared to the FCO approach, the longer coasting distance of the engine start/stop strategy results in decreased fuel consumption without a significant increase in trip time. The FCO strategy performs similarly to the engine-idling strategy and is activated at 4000 m in the Chongqing route (Fig. 6). However, the existing engine drag torque caused by the terminated fuel injection compromises the improvement in performance.

Remark 2 (Weights α and β): In Fig. 5, increasing weight β results in better performance for FCO and engine start/stop coasting methods under Chongqing and Wuhan slope profiles, as more emphasis is placed on fuel consumption in the cost function. When weight α is decreased in the FCO method (Fig. 7), more frequent FCO actions occur, leading to decreased fuel consumption but increased trip time. The cost for restarting the engine in the dynamic equation (17) is formulated to avoid frequent engine start/stop switches, providing a fair evaluation of overall performance while eliminating driving discomfort.

IV. MPC-Based Eco-Coasting Framework

In this section, an online control design framework for the eco-coasting strategy based on MPC is proposed. Based on the analysis in Section III-E, the engine start/stop mechanism is adopted as the best coasting mechanism for the eco-coasting controller. To mitigate frequent engine start/stop behaviors, a new constraint is incorporated in the MPC formulation. Moreover, an integrated branch-and-bound and SQP algorithm is proposed to enable the proposed eco-coasting controller for real-world applications.

A. Model Predictive Control

In control systems subject to constraints on inputs and states, MPC is a technique that embeds optimization within feedback

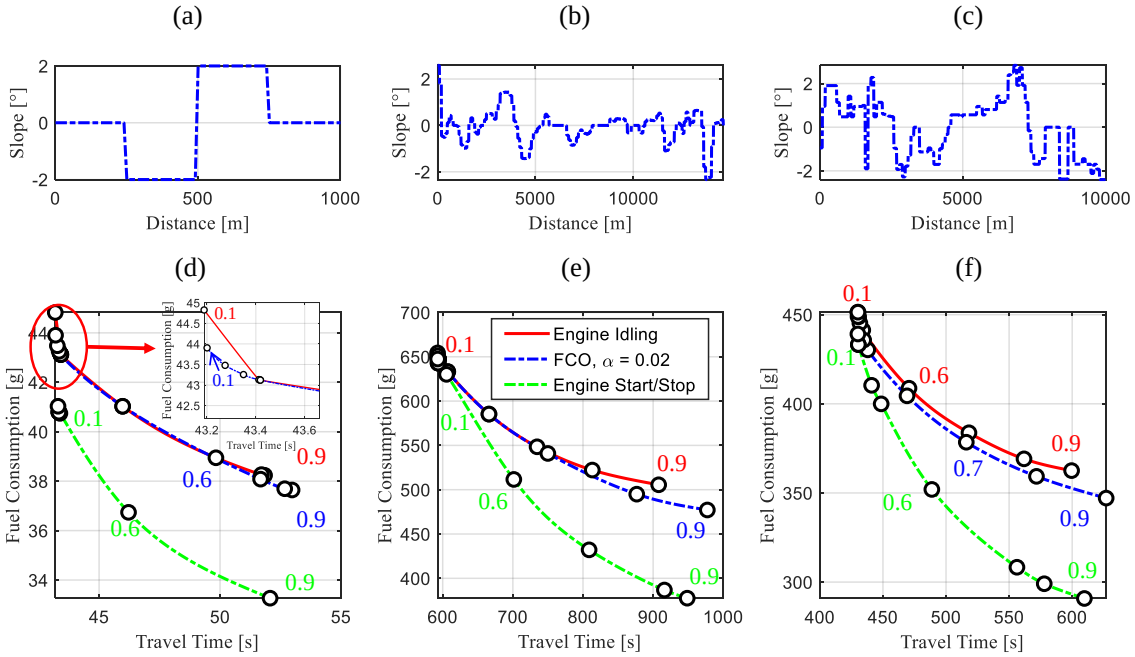

Figure 5. DP results for various coasting methods with corresponding Pareto Front: (a) and (d) Standard uphill-downhill slope profile, (b) and (e) Wuhan slope profile, and (c) and (f) Chongqing slope profile.

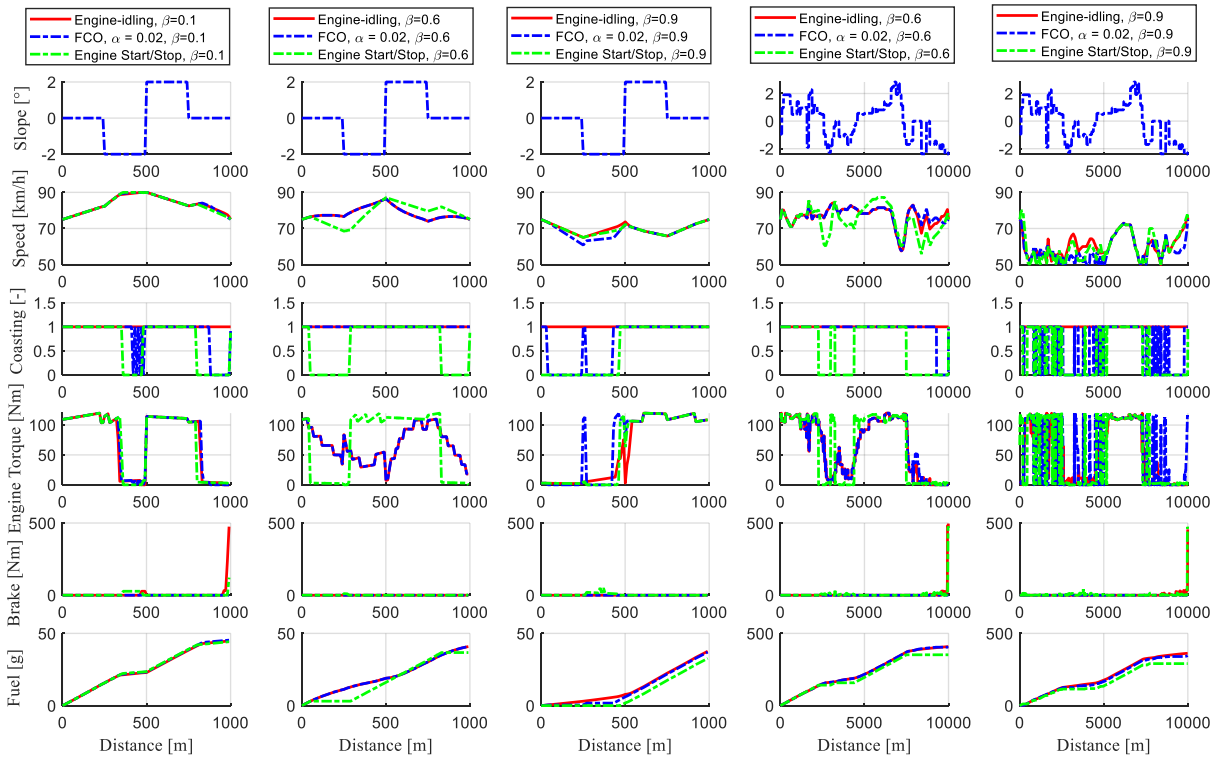

Figure 6. DP results for standard uphill-downhill route (left three columns) and Chongqing route (right two columns)

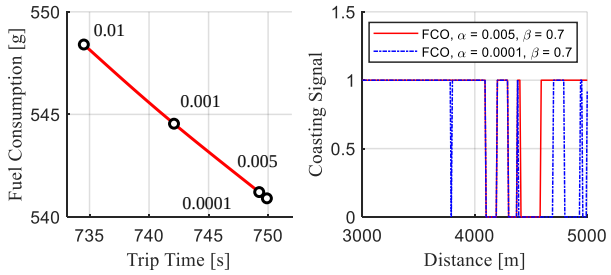

Figure 7. The performance trade-off with the FCO coasting method by varying α (left). FCO signal with different α under the Wuhan slope profile (right).

Algorithm 1 : MIMPC with Minimum-Off Constraints

Input: Initialize $v_{0|k}$, C and $d_{history}$

Output: The augmented constraints added to the original MIMPC

for $j = 1, \ldots, N_h$ **do**
  for $i = 1, \ldots, (d_{\text{dim}} + N_h)$ **do**
    $C := [C, \tau(k : \min(N_h, i + d_{\text{dim}} - 1)) \leq \tau(i) - \tau(i-1)]^T$;
  end
  Impose constraints vector C to original MIOCP; Calculate $T_e \in \mathcal{R}^{N_h}$, $T_b \in \mathcal{R}^{N_h}$, $d \in \mathcal{R}^{N_h}$; Update $d_{history} := \left[d_{j-d_{\min}}, \ldots, d_{k-1}, d_{1|k}\right]^T$;
end

[33]. MPC determines the control action by solving an open-loop optimal control problem over a finite horizon online at each discrete instant. Unlike the cost function in DP, which provides offline results that are unsuitable for the eco-coasting control system, the eco-coasting system is a sub-system of the predictive cruise control system, as shown in Fig. 1, and must be designed to track the reference speed that represents the driver's preference and speed limits. Therefore, we formulate the eco-coasting controller in the MPC scheme to minimize fuel consumption over the horizon while tracking a time-varying trajectory v_{ref} that represents the driver's input during cruise control. Here, $v(i|k)$ denotes the value of variable v at distance $k+i$ when making a prediction at the current location k. We define the MIMPC for the engine start/stop method over a finite-distance horizon (N_h) as follows:

$$\min_{T_e(\cdot|k), T_b(\cdot|k), d(\cdot|k)} \sum_{i=0}^{N_h} (\beta_m \cdot (M_f(i|k)) + (1-\beta_m) \cdot (v(i|k) - v_{\text{ref}})^2) \Delta s, \tag{25}$$

subject to the system dynamics and operational constraints:

$$\begin{aligned}
&v(i+1|k) = v(i|k) \\
&+ \frac{1}{m_{\text{eff}} v(i|k)} \left[F_t - F_r\right] \Delta s - \Delta v(i|k), i = 0 : N_h - 1 \\
&50km/h \leq v(i|k) \leq 90km/h, i = 0 : N_h \\
&0Nm \leq T_e(i|k) \leq 120Nm \cdot d(i|k), i = 0 : N_h - 1 \\
&0Nm \leq T_b(i|k) \leq 500Nm \cdot (1 - d(i|k)), i = 0 : N_h - 1 \\
&d(i|k) \in \{0, 1\}, i = 0 : N_h - 1 \\
&v(0) = 75km/h,
\end{aligned} \tag{26}$$

where β_m is the weighting parameter that affects the trade-off between fuel consumption and tracking accuracy of the eco-coasting controller. Different from the DP formulation, the terminal speed restriction is removed as the speed tracking is considered over the horizon as a soft constraint. The removal of terminal speed constraints will provide more flexibility for fuel efficiency optimization.

To predict and optimize the future behavior of the vehicle powertrain system, the proposed eco-coasting controller employs the engine start/stop coasting model. However, the use of an integer control variable for engine start/stop maneuver results in a MIMPC problem. To address the excessive switch problem in the formulation, the following mixed-integer linear inequalities can express operational constraints on the minimum number of steps for which an engine must remain off:

$$\delta(\tau) \leq 1 - (\delta(j-1) - \delta(j)) \tag{27}$$

with $\tau = j+1, \ldots, \min(j + d_{\min} - 1, N)$, $d_{\min} = 4$ represents the operational constraints on minimum off steps, $j = 2, \ldots, N + d_{\min}$. Let the extended state be represented by the vector $\delta := [d_{\text{history}}, d_{\text{current}}]^T$, where d_{history} is the vector of the previous binary variables with dimension $d_{\min} \times 1$ as

$$d_{\text{history}} := \left[d_{(k-d_{\min}-1)}, \ldots, d_{k-1}\right]^T. \tag{28}$$

d_{current} is the row vector of the current binary variables with dimension $N_h \times 1$ as

$$d_{\text{current}} := \left[d_{1|k}, \ldots, d_{N_h|k}\right]^T. \tag{29}$$

Algorithm 1 presents the implementation of the mixed integer linear inequalities in the MPC formulation. For additional details regarding these constraints, please refer to the works by Parisio *et al.* in [24] and [34].

B. Characteristics Analysis of OCPs

Through the analysis of the optimal control problem, the characteristics that can be used to tailor the solver construction are listed as follow:

1) Parameterized Road Grade Information: The formulated optimal control problem parameterizes the road grade information obtained from the digital map. The tailored solver should solve the fuel optimal control problem to obtain the optimal control sequence with the parameterized road grade information.

2) Nonlinear Equality Constraints: The optimal control problem has nonlinear dynamic equation constraints. To discretize the optimal control problem using the direct multiple shooting method, the nonlinear dynamic equation constraints will result in a large, sparse problem.

3) Integer Control Variables: The engine start/stop maneuver is an integer control variable. As a result, the MPC-based eco-coasting controller should solve a mixed integer nonlinear programming problem at each sampling instance. Furthermore, operational constraints, such as the minimum number of steps for which an engine must be kept off, should be considered over the prediction horizon.

Algorithm 2: Mixed Integer Nonlinear Programming Algorithm based on Branch and Bound and SQP

Input: Initial guess of co-state variables, slack variables, and upper bound

Output: Engine torque, brake torque, coasting variables T_e^*, T_b^*, z^*

```
Solving the relaxed NLP with SQP by relaxing all the binary variables;
while the set of the waiting binary variables is not empty do
    Solving the relaxed NLP with SQP by relaxing all the binary variables ;
    repeat
        Update the co-state variables, slack variables, and upper bound ;
        repeat
            Calculate the sub-QP;
        until Satify the terminal condition of QP or maximum number of iterations exceeded;
        Number of iterations + 1 ;
    until Satify the terminal condition of SQP or maximum number of iterations exceeded;
end
```

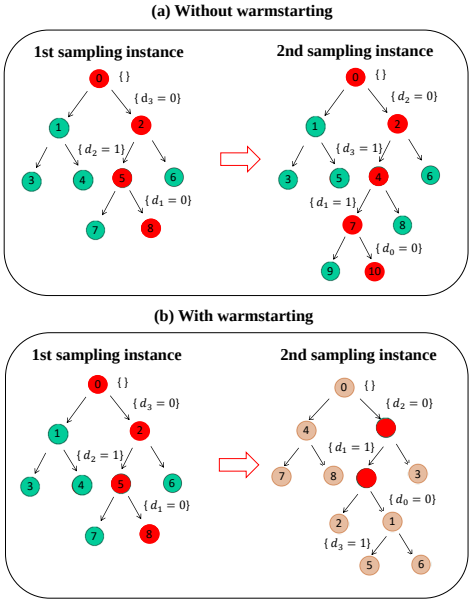

Figure 8. Effect validation of the warmstarting strategy for eco-coasting. Index in the circle denotes the order of node which is solved

C. Tailored Mixed-integer Programming Algorithm for the Eco-coasting Strategy

To demonstrate the implementation feasibility of the proposed eco-coasting strategy, a tailored mixed-integer programming algorithm is proposed in this section. A computation strategy composed of the branch-and-bound method and sequential quadratic programming (BBSQP) is proposed by leveraging the characteristics analyzed in Section IV-B.

To solve the MINLP problem, a branch-and-bound strategy is used to decompose the integer part from the original problem. Initially, all integer restrictions are relaxed into a range of 0 to 1, and the resulting NLP relaxation is solved. If all the fuel cut-off signals over the prediction horizon take a binary value at the solution, the MINLP is solved. Otherwise, one of the non-binary binary variables is chosen and branched to create two new NLP problems with additional constraints. These generated NLP problems are added to the candidate queue, and the procedure is repeated until the queue is empty. The whole branch-and-bound procedure can be depicted as a binary tree, with nodes representing the NLP problem and edges indicating the added constraints. At each node, SQP is used to solve the NLP relaxation problem. For more details on the SQP, see Appendix A. The sub-QP problem is solved using the FBstab solver, which is known for its numerical robustness, ability to exploit sparsity, ease of warmstarting, and infeasibility detection capabilities [35]. This solver, coupled with infeasibility detection, enables an early-branching rule to be implemented in the branch-and-bound method, leading to reduced computation complexity. The proposed BBSQP algorithm is shown in Algorithm 2.

To select the next sub-problems in the branch-and-bound method, various criteria can be used, such as depth-first,

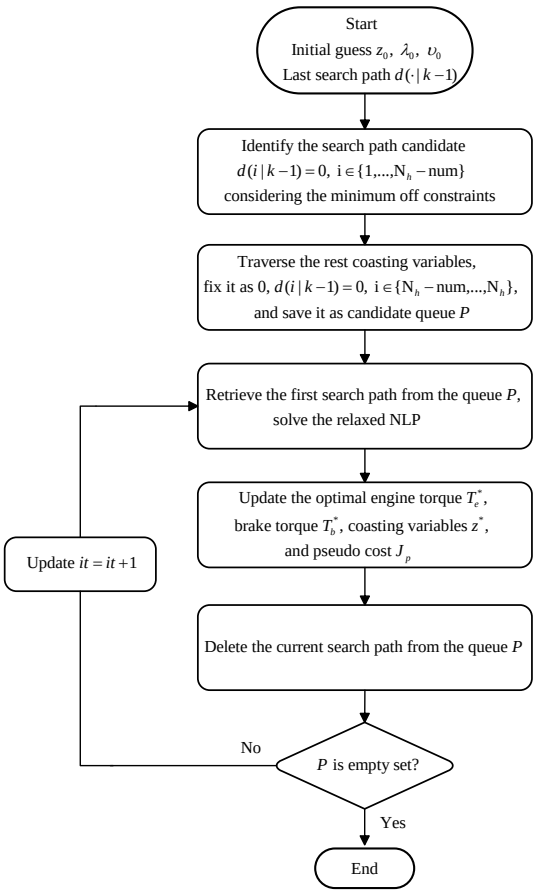

Figure 9. Flowchart of the minimum off constraints speedup strategy for BBSQP algorithm

breadth-first, branch on the best/worst cost solution. Non-binary variables are often present in the obtained optimal solution of the NLP relaxation, and two common ways to select the branching variable are based on the most/least fractional variable. These selection strategies can significantly impact computational time. In this study, the branch on the best cost solution and the branch on the most fractional variable are chosen as the optimized candidate selection strategies for the eco-coasting problem based on offline simulation performance. Additionally, two speedup methods are proposed and incorporated into the eco-coasting controller to further ease the computation of the BBSQP algorithm.:

1) Warmstarting of the MIMPC: To mitigate computation overhead, the sequential nature of the problem allows taking the solution of the last OCP as a starting point for the current one. In the eco-coasting problem using the branch-and-bound method, the search path of the previous sampling instance's branch-and-bound tree is saved and propagated to the next sampling instance.

The procedure of warmstarting for the eco-coasting problem is illustrated with 5 predictive steps in Fig. 8. In this study, the convergence tolerance of SQP, initial slack variables, maximum node numbers of the branch-and-bound method, and integer tolerance are set to $tol = 10\mathrm{e}-4$, $s = 10$, $maxNodes = 100000$, and $intTol = 10\mathrm{e}{-3}$. As shown in Fig. 8, the optimal path at the first sampling step is $d_3 = 0 \rightarrow d_1 = 1 \rightarrow d_0 = 0$. Without the warmstarting strategy, this path information cannot be used at the next sampling step, so the second and fourth nodes would be solved repeatedly. With warmstarting, however, the optimal path from the previous sampling step is propagated to the current one, after ignoring the first control action of the engine start/stop sequence. All the leaf nodes of this path are then solved in order, from the bottom layer to the upper layer. As a result, only 8 NLP relaxations are solved to find the optimal engine start/stop sequence, as opposed to solving all nodes in the branch-and-bound tree.

2) Minimum off constraints: To reduce the number of "useless" branches, the tree search process incorporates the operational constraints of engine start/stop. Inspired by the mixed integer linear inequalities in Section IV-A, an augmented vector is formed by concatenating the history engine start/stop signals d_{history} and engine start/stop signals over the horizon d_{current}. If there is an engine start/stop activation signal in d_{history}, the number of consecutive engine start/stop activation signals num from the back to the front is calculated. Subsequently, the first $N_h - num$ variables over the horizon d_{current} are fixed to 0, which keeps the engine start/stop signal active. To avoid frequent switches of engine start/stop actions over the horizon, it is assumed that the signal can only switch once in the prediction horizon. Once the activation variables are determined, other variables in the prediction horizon are traversed as switch variables from front to back. The value of the variable after the switch variable must be the same as the value of the switch variable. Then, the location of the switch variable in the predicted time domain is found. However, it should be noted that this speedup strategy depends on the prediction-horizon length, resulting in a deterministic computational footprint, as the number of exploration nodes in the horizon is essentially the same as the prediction steps. The flowchart of this speedup strategy is illustrated in Fig. 9.

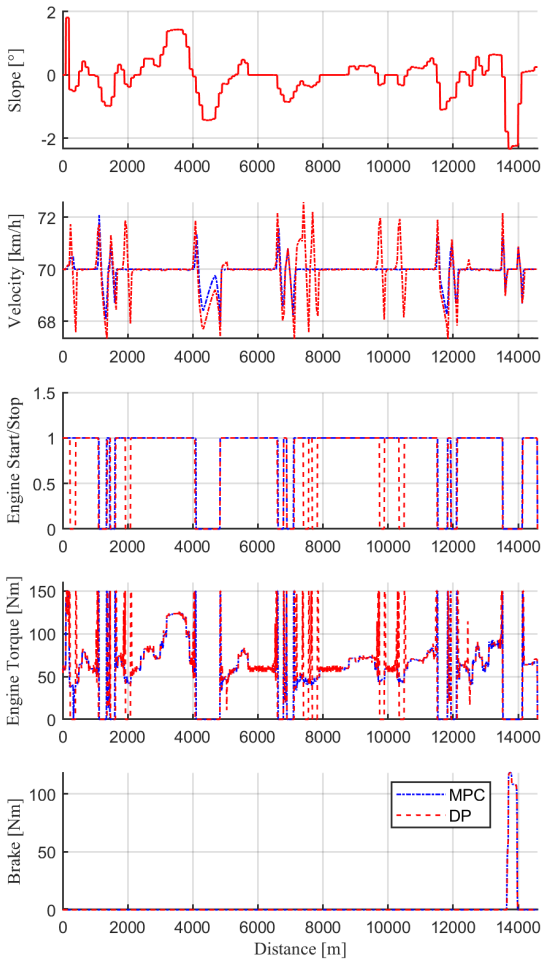

Figure 10. Simulation results comparison with engine start/stop method with the Wuhan slope profile: DP vs MPC

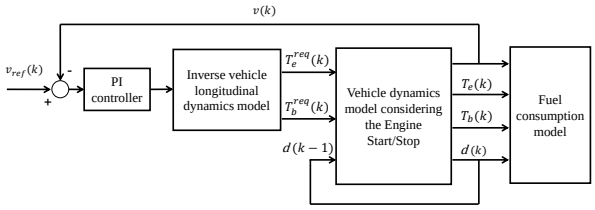

Figure 11. Control architecture for the rule-based engine start/stop mechanism. T_e^{req} is the required engine torque, T_b^{req} is the required brake torque, $d(k-1)$ is the engine start/stop maneuver at the last step.

V. Performance Evaluation and Discussion

In this section, we validate the effectiveness of the proposed eco-coasting controller in two steps. First, the MPC-based eco-coasting approach is evaluated with the same Wuhan route in Section III and compared with the globally optimal DP solution. Secondly, extensive simulations are performed to compare the eco-coasting controller with a rule-based controller. Finally,

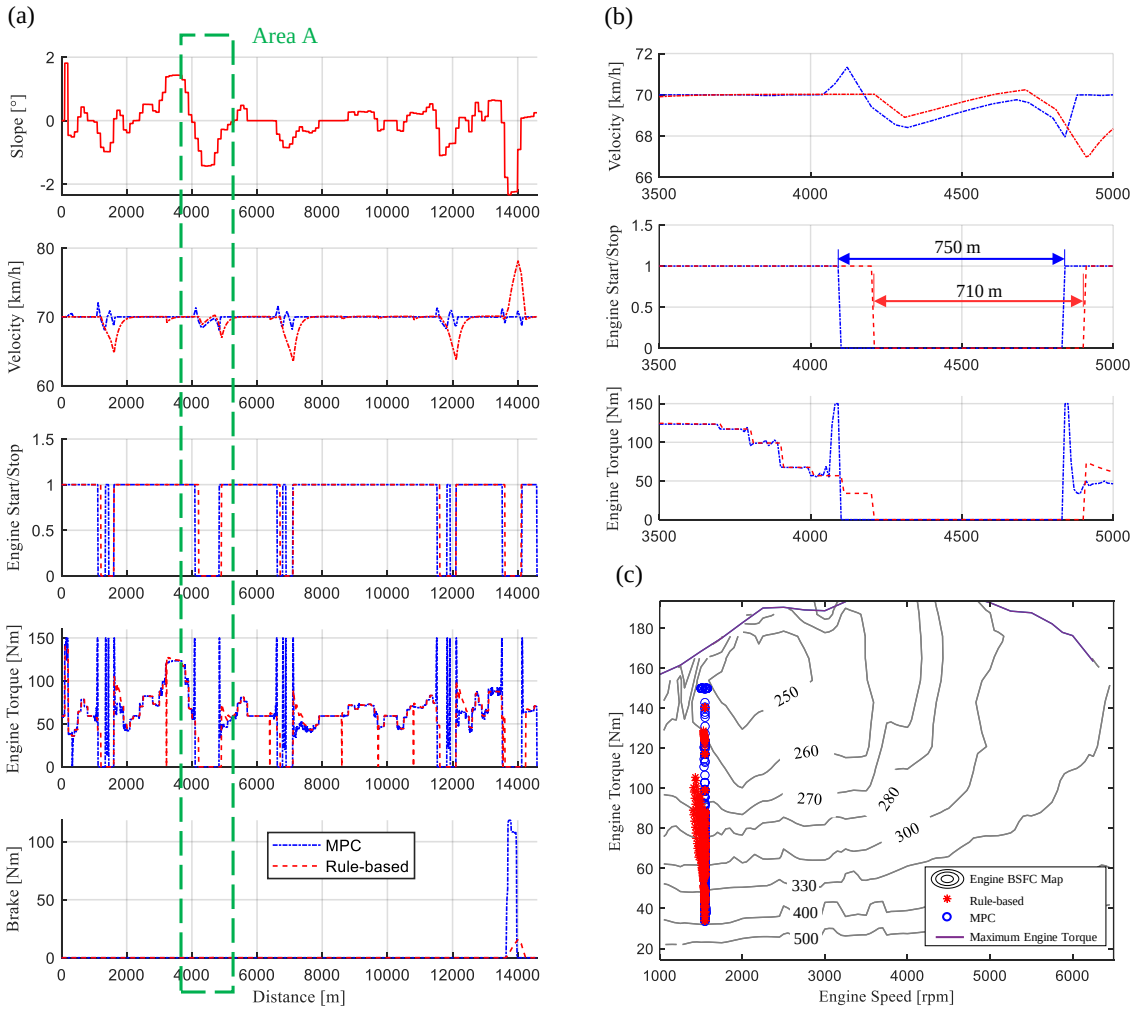

Figure 12. Simulation results comparison of the MPC-based eco-coasting controller and the rule-based method on varying slope conditions. (a) Results over the Wuhan driving cycle. (b) Detailed views of the simulation results in Area A of subfigure (a). (c) Engine operating points when the engine is turned on.

discussions are made regarding the length of the prediction horizon concerning the use of the eco-coasting controller in real-world applications.

Table 3
PERFORMANCE COMPARISON WITH ENGINE START/STOP APPROACH: DP ($\beta_m = 0.5$) VS MPC ($\beta_m = 0.5$)

Controller	Fuel consumption	Trip time
MPC	541.9 g	751.6 s
DP	533.2 g	751.0 s
Comparison	+1.63 %	+0.04 %

A. Performance Comparison with DP

To validate the performance of the MPC-based eco-coasting controller in comparison to the DP solution, we apply the proposed controller to a realistic driving cycle in Wuhan (Fig.4), with a cruise speed of 70 km/h in consideration of the highway speed limit. For a fair comparison, we solve the same optimal control problem for the entire trip using DP, as formulated in equations (25) and (26). Table 3 summarizes the energy consumption and trip time obtained using both controllers. The results show that both controllers drive the vehicle to the destination within the same trip time by following the reference speed, with the MPC-based eco-coasting controller achieving energy efficiency close to the globally optimal solution. This is because, as shown in Fig. 10, the MPC replicates almost every engine switched-off action of the globally optimal solution but may miss some due to local optima and switch constraints.

B. Performance Comparison with Rule-based Engine Start/Stop Method on Varying Slope Conditions

To further demonstrate the effectiveness of the MPC-based eco-coasting controller, we propose a rule-based engine start/stop method. In situations where controller hardware capability is limited, a rule-based approach is often preferred because it can achieve comparable performance with low computational complexity. The control architecture, as shown in Fig. 11, employs a PI controller to track the cruise speed set by the driver, followed by an inverse vehicle longitudinal dynamics model to calculate the required engine torque and

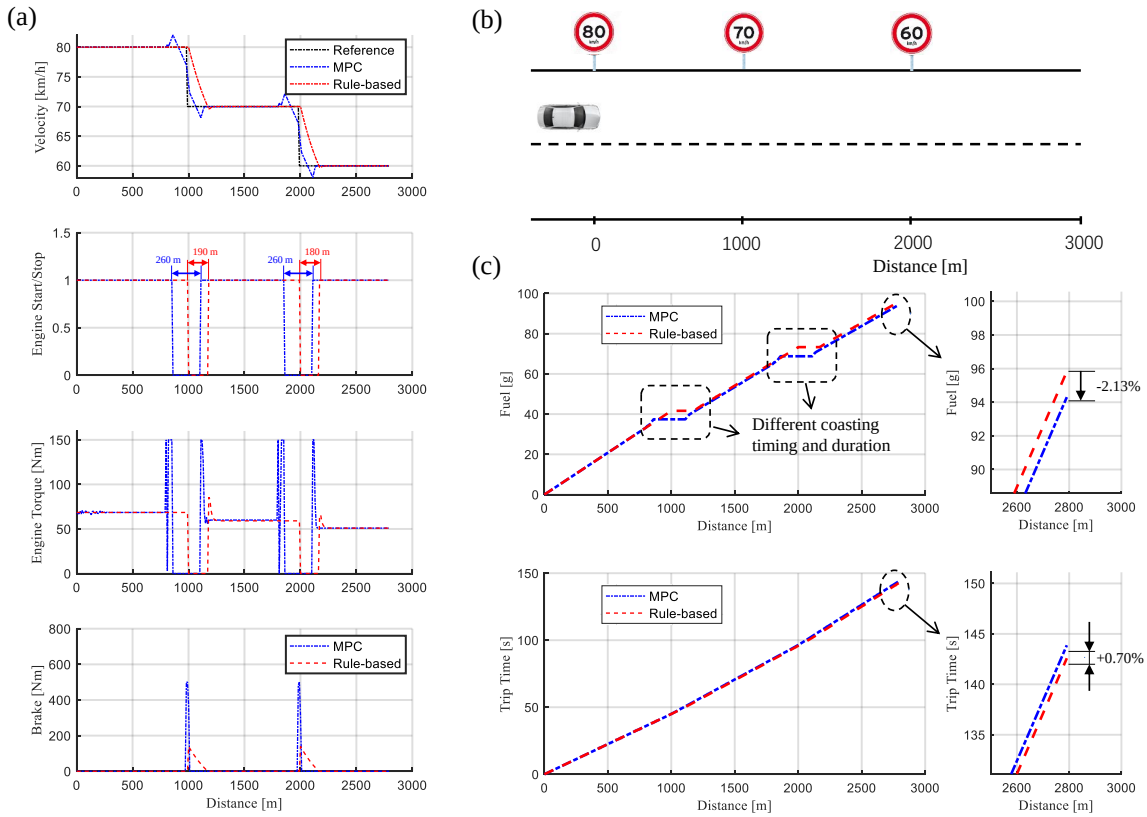

Figure 13. Simulation results comparison of the MPC-based eco-coasting controller and the rule-based method on varying speed limit conditions. (a) Simulation results illustration. (b) Simulation setup illustration. (c) Performance comparison.

brake torque. Finally, the engine start/stop maneuver is derived based on a rule that switches off the engine on a downhill stretch when the current road grade is less than a certain threshold (-0.57°) and the current speed is higher than a threshold (60 km/h) simultaneously. If the engine is turned off under these conditions, the engine turn-off signal will hold for 10 discretization steps to avoid frequent switches [36]. The operational constraints on minimum stop steps in this study are tuned offline to balance tracking accuracy and fuel consumption. The simulation is also performed on the Wuhan driving cycle, and the cruise speed is set as 70 km/h. As shown in Table 4, compared with the rule-based engine start/stop method, the MPC-based eco-coasting controller achieves 5.95% fuel-saving performance with even a slightly shorter trip time.

Table 4
PERFORMANCE COMPARISON WITH ENGINE START/STOP APPROACH: MPC ($\beta_m = 0.5$) VS RULE-BASED METHOD.

	Fuel consumption	Trip time
MPC	541.9g	751.6 s
PI(P=0.1,I=0.00001)	576,2g	754.3 s
Comparison	-5.95%	-0.36 %

The superior performance of the MPC-based eco-coasting controller compared to the rule-based method can be attributed to two reasons. Firstly, the MPC-based controller can adapt coasting to varying slopes in real-time using its forecasting feature, thereby increasing the coasting distance. For instance, as illustrated in Fig. 12(b), the controller increases the vehicle velocity in advance before a steep downhill, allowing the vehicle to achieve a longer coasting distance of 750 m compared to that of the rule-based method's 710 m. Longer coasting distance means longer engine off duration which results in better fuel economy. Consequently, the eco-coasting controller achieves higher fuel efficiency without compromising speed-tracking performance. Secondly, in addition to the engine turn-off condition, the MPC controller can optimize the engine work area adapted to the road slope prediction, as shown in Fig. 12 (c). The increased engine torque of the MPC controller falls within the engine's economical range, resulting in improved fuel economy compared to the rule-based method with the PI controller.

C. Performance Comparison with Rule-based Engine Start/Stop Method on Varying Speed Limit Conditions

The advanced performance of the MPC-based eco-coasting controller is further elaborated on using a new simulation setup in this study. The reference speed is adapted to the varying speed limit on the urban expressway, as shown in Fig. 13 (b). The activation condition for the rule-based method is updated when the required engine torque is zero. Fig. 13 (a) shows that the MPC-based eco-coasting controller increases its speed in advance before the drop of the reference speed

to gain a longer coasting distance. The different coasting timing and duration of the MPC-based eco-coasting controller and the rule-based method contribute to the final fuel-saving performance (2.13% reduction) without compromising the trip time performance (Fig. 13 (c)).

D. Discussion on the Length of the Prediction Horizon

In this study, the impact of the prediction horizon length on the performance of the eco-coasting controller is analyzed. The simulations are conducted using MATLAB R2019a on an AMD Ryzen 5 2600X 3.60-GHz with 16.0-GB RAM. As depicted in Fig. 14, the fuel consumption reduces by 5.10% and 8.71% when the prediction horizon increases from 50 m to 100 m and 200 m, respectively. On the contrary, the trip time increases by 0.60% and 1.02%, respectively. A longer prediction horizon provides more reference speed information to the MPC controller to proactively adjust the coasting timing and duration with respect to the road grade and speed limit. However, the eco-coasting controller's performance does not necessarily improve with a longer prediction horizon, as shown in Fig. 14, where the eco-coasting controller with a 400 m prediction horizon only achieves a slight fuel efficiency improvement, while the computation time increases dramatically. Additionally, a longer prediction horizon makes the MPC-based eco-coasting controller more vulnerable to model mismatch. Fig. 14(d) illustrates the computation time at each sampling instance of the eco-coasting controller with a 200 m prediction horizon. The overall computation time is below 0.1 seconds over the Wuhan driving cycle, indicating that the eco-coasting controller can be performed with a 10 Hz control cycle, sufficient for the highway cruise control scenario without a vehicle in front.

VI. Conclusion

In this article, we investigate the eco-coasting control of gasoline vehicles under cruise conditions. To develop an optimal control strategy feasible for real-time application, an MPC-based eco-coasting controller that optimizes the engine torque, brake torque, and coasting signal simultaneously is proposed. The key findings of this research are listed as follows:

- Based on the results of the offline evaluation, it was determined that the engine start/stop method is the most effective coasting method for the eco-coasting controller when utilizing look-ahead information, outperforming both the engine idling method and fuel cut-off method;
- Integrated the branch-and-bound method and sequential quadratic programming is a promising way to solve the mixed integer programming problem of the eco-coasting controller numerically at each MPC iteration. The tailored speedup strategies based on the characteristics of the optimal control problem can guarantee real-time implementation feasibility of the eco-coasting controller on computing power-limited ECUs;
- Based on the simulation results, it was observed that the MPC-based eco-coasting controller can achieve near-optimal fuel efficiency performance when compared to globally optimal solutions. Furthermore, the proposed controller outperforms a rule-based engine start/stop method with a longer coasting distance leveraging the predictive feature.

Future work will focus on the experimental validation of the proposed eco-coasting controller on the test-bed vehicle. While the computational efficiency of the proposed BBSQP solver was studied and confirmed, a convergence proof of the BBSQP solver with different speedup strategies is also a subject left for future research.

Appendix A
Sequential quadratic programming

Slack variables $\dot{s} = [\dot{s}_1 \cdots \dot{s}_{N_h}]^T \in \mathbb{R}^{N_h}$ is integrated into the inequality constraints to increase the feasible set of the NLP. The state variables are $x = [v_1 \cdots v_{N_\star}]^T \in \mathbb{R}^{N_h}$ and the control variables are $u = \begin{bmatrix} T_{e,0} & T_{b,0} & z_0 \cdots T_{e,N_h-1} & T_{b,N_h-1} & z_{N_h-1} \end{bmatrix} \in \mathbb{R}^{N_h \times 3}$. We defined $\dot{z} = \begin{bmatrix} u^T x^T \dot{s}^T \end{bmatrix}^T$ to denote the collected primal variables. Then, the eco-coasting problem is cast as an NLP with generalized formulation,

$$\begin{aligned} &\min_{\dot{z}} f(\dot{z}) \\ \text{s.t.} \quad &g(\dot{z}) = 0 \\ &c(\dot{z}) \leq 0, \end{aligned} \tag{30}$$

The Lagrangian for this problem is

$$L(\dot{z}, \lambda, v) = f(\dot{z}) + \lambda^T g(\dot{z}) + v^T c(\dot{z}) \tag{31}$$

where $\lambda \in \mathbb{R}^m$ and $v \in \mathbb{R}^q$ are dual variables. At the kth iteration, the sub-QP problem have the form

$$\begin{aligned} \min_{\Delta \dot{z}} \quad &\frac{1}{2} \Delta \dot{z}^T H_k \Delta \dot{z} + r_k^T \Delta \dot{z} \\ \text{s.t. } &G_k \Delta \dot{z} + g_k = 0 \\ &C_k \Delta \dot{z} + c_k \leq 0 \end{aligned} \tag{32}$$

where $H_k = \nabla^2_{\dot{z}} L(\dot{z}_k, \lambda_k, v_k)$, $r_k = \nabla_{\dot{z}} L(\dot{z}_k)$, $G = \nabla_{\dot{z}} g(\dot{z}_k)$, $g_k = g(\dot{z}_k)$, $C_k = \nabla_{\dot{z}} c(\dot{z}_k)$, and $c_k = C(\dot{z}_k)$. The SQP iteration will be finished when the natural residual

$$F_{NR}(x) = \begin{bmatrix} \nabla_{\dot{z}} \mathrm{L}(\dot{\mathrm{z}}, \lambda, v) \\ g(\dot{z}) \\ \min(-c(\dot{z}), v) \end{bmatrix} \tag{33}$$

reaches the convergence tolerance. Note that the Hessian/Jacobian matrices of the Lagrangian are generated and assembled using MATLAB's symbolic toolbox. A scaled identity matrix is added to the Hessian matrices of the Lagrangian to ensure its positive semidefinite property and then guarantee the sub-QP problem is convex.

Acknowledgment

Y. Yan acknowledges the support from the Chinese Scholarship Council that made this work possible. This work was done when he was a visiting Ph.D. student in the Department of Naval Architecture and Marine Engineering, University of Michigan, Ann Arbor, MI 48109 USA. The work of J. L. Hong, B. Z. Gao and H. Chen was supported by the National Natural

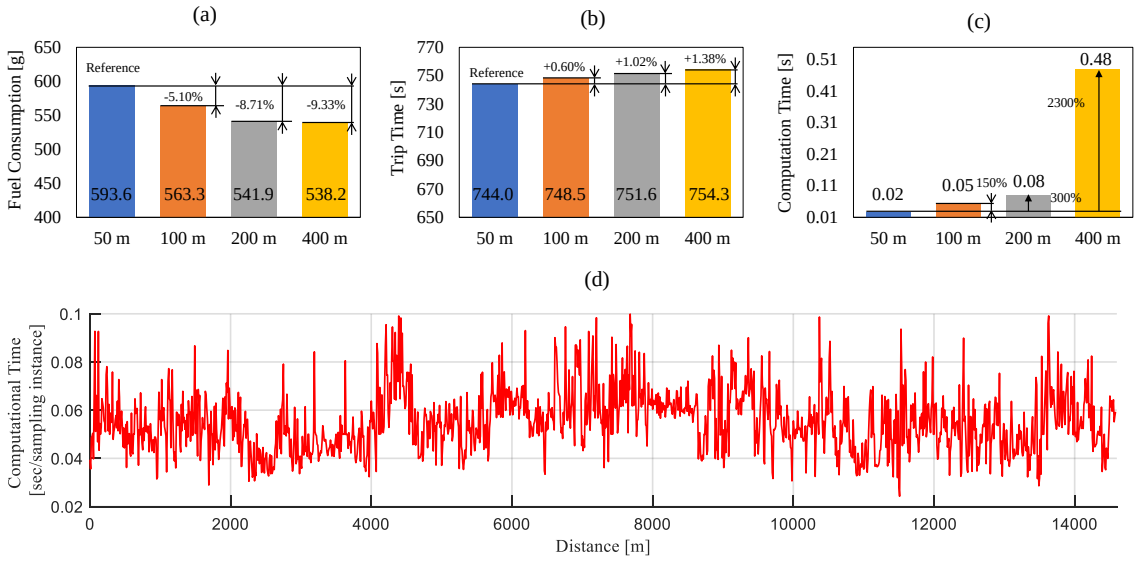

Figure 14. Effect of increasing the prediction horizon on the engine start/stop method. (a) Fuel consumption. (b) Trip time. (c) Average computation time. (d) Computation time at each sampling instant with a 200 m prediction horizon.

Science Foundation of China No.62003244, the Foundation of State Key Laboratory of Automotive Simulation and Control No.20210210, and in part by Jilin provincial Science & Technology Department No.20200301011RQ. The authors would like to thank Dominic Liao-McPherson for the advice about the FBstab solver.

REFERENCES

[1] G. Li, D. Görges, and M. Wang, "Online optimization of gear shift and velocity for eco-driving using adaptive dynamic programming," *IEEE Transactions on Intelligent Vehicles*, vol. 7, no. 1, pp. 123–132, 2021.

[2] Y. Jia, T. Saito, Y. Itoh, Y. Nukezhanov, and D. Görges, "Energy-optimal adaptive cruise control in time domain based on model predictive control," *IFAC-PapersOnLine*, vol. 51, no. 31, pp. 846–853, 2018.

[3] Y. Jia and D. Görges, "Energy-optimal adaptive cruise control based on hybrid model predictive control with mixed-integer quadratic programming," in *2020 European Control Conference (ECC)*. IEEE, 2020, pp. 686–692.

[4] C. F. Salgueiredo, O. Orfila, G. Saint Pierre, P. Doublet, S. Glaser, S. Doncieux, and V. Billat, "Experimental testing and simulations of speed variations impact on fuel consumption of conventional gasoline passenger cars," *Transportation Research Part D: Transport and Environment*, vol. 57, pp. 336–349, 2017.

[5] S. E. Li, K. Deng, Y. Zheng, and H. Peng, "Effect of pulse-and-glide strategy on traffic flow for a platoon of mixed automated and manually driven vehicles," *Computer-Aided Civil and Infrastructure Engineering*, vol. 30, no. 11, pp. 892–905, 2015.

[6] A. Balluchi, M. Di Benedetto, C. Pinello, C. Rossi, and A. Sangiovanni-Vincentelli, "Cut-off in engine control: a hybrid system approach," in *Proceedings of the 36th IEEE Conference on Decision and Control*, vol. 5. IEEE, 1997, pp. 4720–4725.

[7] Y. Katsumata, S. Segawa, K. Adachi, A. Higashimata, and Y. Ochi, "Development of a slip speed control system for a lock-up clutch (part ii)," SAE Technical Paper, Tech. Rep., 2008.

[8] H. Koch-Groeber and J. Wang, "Criteria for coasting on highways for passenger cars," SAE Technical Paper, Tech. Rep., 2014.

[9] J. Lee, "Vehicle inertia impact on fuel consumption of conventional and hybrid electric vehicles using acceleration and coast driving strategy," Ph.D. dissertation, Virginia Tech, 2009.

[10] J. Bishop, A. Nedungadi, G. Ostrowski, B. Surampudi, P. Armiroli, and E. Taspinar, "An engine start/stop system for improved fuel economy," SAE technical paper, Tech. Rep., 2007.

[11] P. Griefnow, J. Andert, and D. Jolovic, "Next-generation low-voltage power nets impacts of advanced stop/start and sailing functionalities," *SAE International Journal of Fuels and Lubricants*, vol. 10, no. 2, pp. 556–573, 2017.

[12] P. Griefnow, J. Andert, F. Xia, S. Klein, P. Stoffel, M. Engels, and D. Jolovic, "Real-time modeling of a 48v p0 mild hybrid vehicle with electric compressor for model predictive control," *SAE Tech. Paper*, 2019.

[13] C. Sohn, J. Andert, and D. Jolovic, "An analysis of the tradeoff between fuel consumption and ride comfort for the pulse and glide driving strategy," *IEEE Transactions on Vehicular Technology*, vol. 69, no. 7, pp. 7223–7233, 2020.

[14] R. Varnhagen, "Electronic horizon: A map as a sensor and predictive control," SAE Technical Paper, Tech. Rep., 2017.

[15] S. Choi, K. Ko, and I. Jeung, "Optimal fuel-cut driving method for better fuel economy," *International Journal of Automotive Technology*, vol. 14, no. 2, pp. 183–187, 2013.

[16] N. Mueller, S. Strauss, S. Tumback, G.-C. Goh, and A. Christ, "Next generation engine start/stop systems: "free-wheeling"," *SAE International Journal of Engines*, vol. 4, no. 1, pp. 874–887, 2011.

[17] E. Hellström, J. Åslund, and L. Nielsen, "Design of an efficient algorithm for fuel-optimal look-ahead control," *Control Engineering Practice*, vol. 18, no. 11, pp. 1318–1327, 2010.

[18] E. Hellström, M. Ivarsson, J. Åslund, and L. Nielsen, "Look-ahead control for heavy trucks to minimize trip time and fuel consumption," *Control Engineering Practice*, vol. 17, no. 2, pp. 245–254, 2009.

[19] A. Sciarretta, G. De Nunzio, and L. L. Ojeda, "Optimal ecodriving control: Energy-efficient driving of road vehicles as an optimal control problem," *IEEE control systems magazine*, vol. 35, no. 5, pp. 71–90, 2015.

[20] D. V. Ngo, "Gear shift strategies for automotive transmissions," *Ph.D. Thesis*, 2012.

[21] G. Li and D. Goerges, "Hybrid modeling and predictive control of the power split and gear shift in hybrid electric vehicles," in *2017 IEEE Vehicle Power and Propulsion Conference (VPPC)*. IEEE, 2017, pp. 1–6.

[22] F. Yan, J. Wang, and K. Huang, "Hybrid electric vehicle model predictive control torque-split strategy incorporating engine transient characteristics," *IEEE transactions on vehicular technology*, vol. 61, no. 6, pp. 2458–2467, 2012.

[23] S. Esmaeili, S. Jadid, A. Anvari-Moghaddam, and J. M. Guerrero, "Optimal operational scheduling of smart microgrids considering hourly reconfiguration," in *2018 IEEE 4th Southern Power Electronics Conference (SPEC)*. IEEE, 2018, pp. 1–6.

[24] A. Parisio, E. Rikos, and L. Glielmo, "Stochastic model predictive control for economic/environmental operation management of microgrids: An experimental case study," *Journal of Process Control*, vol. 43, pp. 24–37, 2016.

[25] B. Mayer, M. Killian, and M. Kozek, "Management of hybrid energy supply systems in buildings using mixed-integer model predictive control," *Energy conversion and management*, vol. 98, pp. 470–483, 2015.
[26] P. Belotti, C. Kirches, S. Leyffer, J. Linderoth, J. Luedtke, and A. Mahajan, "Mixed-integer nonlinear optimization," *Acta Numerica*, vol. 22, pp. 1–131, 2013.
[27] R. Takapoui, N. Moehle, S. Boyd, and A. Bemporad, "A simple effective heuristic for embedded mixed-integer quadratic programming," *International journal of control*, vol. 93, no. 1, pp. 2–12, 2020.
[28] H. Yu, F. Zhang, J. Xi, and D. Cao, "Mixed-integer optimal design and energy management of hybrid electric vehicles with automated manual transmissions," *IEEE Transactions on Vehicular Technology*, vol. 69, no. 11, pp. 12 705–12 715, 2020.
[29] A. Richards and J. How, "Mixed-integer programming for control," in *Proceedings of the 2005, American Control Conference, 2005.* IEEE, 2005, pp. 2676–2683.
[30] P. Hespanhol, R. Quirynen, and S. Di Cairano, "A structure exploiting branch-and-bound algorithm for mixed-integer model predictive control," in *2019 18th European Control Conference (ECC)*. IEEE, 2019, pp. 2763–2768.
[31] S. Leyffer, "Integrating sqp and branch-and-bound for mixed integer nonlinear programming," *Computational optimization and applications*, vol. 18, no. 3, pp. 295–309, 2001.
[32] H. Chu, L. Guo, B. Gao, H. Chen, N. Bian, and J. Zhou, "Predictive cruise control using high-definition map and real vehicle implementation," *IEEE Transactions on Vehicular Technology*, vol. 67, no. 12, pp. 11 377–11 389, 2018.
[33] Z. Li, J. Sun, and S. Oh, "Path following for marine surface vessels with rudder and roll constraints: An mpc approach," in *2009 American control conference*. IEEE, 2009, pp. 3611–3616.
[34] M. Carrión and J. M. Arroyo, "A computationally efficient mixed-integer linear formulation for the thermal unit commitment problem," *IEEE Transactions on power systems*, vol. 21, no. 3, pp. 1371–1378, 2006.
[35] M. R. Amini, H. Wang, X. Gong, D. Liao-McPherson, I. Kolmanovsky, and J. Sun, "Cabin and battery thermal management of connected and automated hevs for improved energy efficiency using hierarchical model predictive control," *IEEE Transactions on Control Systems Technology*, vol. 28, no. 5, pp. 1711–1726, 2019.
[36] D. Chen, M. Huang, and A. G. Stefanopoulou, "Discrete mixed-integer shooting (dmis): Algorithm and application to plug-in hybrid electric vehicle energy management accounting for fuel cranking and actual powertrain efficiency maps," *IEEE Transactions on Control Systems Technology*, 2022.

Yongjun Yan received the B.S. degree in vehicle engineering from the Hefei University of Technology, Hefei, China, in 2016. and the Ph.D. degree in vehicle engineering at Jilin University, Changchun, China, in 2022. He was a Joint Ph.D. Student at the University of Michigan, Ann Arbor, from 2019 to 2021, where he was co-advised by Prof. J. Sun. His current research interests include optimal control and applications in automobile and continuum robots. He is currently a Post-Doctoral Research Fellow at the Chinese University of Hong Kong.

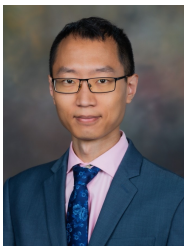

Nan Li received the Ph.D. degree in Aerospace Engineering and the M.S. degree in Mathematics from the University of Michigan, Ann Arbor, MI, USA, in 2021 and 2020, respectively. He is currently an Assistant Professor with the Department of Aerospace Engineering, Auburn University, AL, USA. Prior to joining Auburn University, he was a Postdoctoral Research Fellow at the University of Michigan from 2021 to 2022. His research interests are in optimal control, learning, multi-agent systems, and their applications for connected and automated vehicles.

Jinlong Hong received the B.S. degree in School of Vehicle and Energy from Yanshan University, Qinhuangdao, China, in 2014, the Ph.D. degree in vehicle engineering from Jilin University, Changchun, China, in 2019. He is currently an Assistant Professor at Tongji University. His current research interests include vehicle powertrain optimization control and energy-saving control for intelligent automobiles.

Bingzhao Gao (Member, IEEE) received the B.S. and M.S. degrees in vehicle engineering from Jilin University, Changchun, China, in 1998 and 2002, respectively, the Ph.D. degree in mechanical engineering from Yokohama National University, Yokohama, Japan, and the Ph.D. degree in control engineering from Jilin University in 2009. He is currently a Professor with Tongji University. His current research interests include vehicle powertrain control and vehicle stability control.

Jia Zhang (Member, IEEE) received the Ph.D. degree in control science and engineering from Beijing Institute of Technology, Beijing, China, in 2015. She is currently an Associate Professor with the School of Automation, Beijing Institute of Technology. Her research interest is in multi-objective optimization and decision-making.

Hong Chen (Fellow, IEEE) received the B.S. and M.S. degrees in process control from Zhejiang University, Hangzhou, China, in 1983 and 1986, respectively, and the Ph.D. degree in system dynamics and control engineering from the University of Stuttgart, Stuttgart, Germany, in 1997. In 1986, she joined the Jilin University of Technology, Changchun, China. From 1993 to 1997, she was a Wissenschaftlicher Mitarbeiter with the Institut für Systemdynamik und Regelungstechnik, University of Stuttgart. Since 1999, she has been a Professor with Jilin University, Changchun, and hereafter a Tang Aoqing professor. From 2015 to 2019, she was the Director of the State Key Laboratory of Automotive Simulation and Control, Jilin University. In 2019, she joined Tongji University, Shanghai, China, as a Distinguished Professor. Her current research interests include model predictive control, nonlinear control, and applications in mechatronic systems focusing on automotive systems.

Jing Sun (Fellow, IEEE) is Michael G. Parsons Collegiate Professor of the Naval Architecture and Marine Engineering Department at the University of Michigan. She received her Ph. D degree from the University of Southern California in 1989 and her B.S. and M.S. degrees from the University of Science and Technology of China. From 1989-1993, she was an assistant professor in the Electrical and Computer Engineering Department at Wayne State University. She joined Ford Research Laboratory in 1993, working in the Powertrain Control Systems Department. After spending almost 10 years in the industry, she returned to academia and joined the faculty of the College of Engineering at the University of Michigan in 2003. Her research interests include modeling, control, and optimization of dynamic systems with applications to marine and automotive systems. Her current research focuses on real-time optimization and decision-making for energy and transportation systems. She holds 44 U.S. patents and has published over 300 peer-reviewed journal and conference papers. She co-authored the textbook "Robust Adaptive Control," which received over 7500 citations. She is a Fellow of the National Academy of Inventors, IEEE, IFAC, and the Society of Naval Architects and Marine Engineers. She is a recipient of the 2003 IEEE Control System Technology Award.

Ziyou Song is an Assistant Professor with the Department of Mechanical Engineering at the National University of Singapore. He received B.E. degree (with honours) and Ph.D. degree (with highest honours) in Automotive Engineering from Tsinghua University, Beijing, China, in 2011 and 2016, respectively. After graduation, he worked as a Research Scientist at Tsinghua University from 2016-2017. From 2017 to 2019, he worked as a Postdoctoral Research Fellow at the University of Michigan, Ann Arbor, where he was also an Assistant Research Scientist/Lecturer from 2019 to 2020. Prior to joining NUS, he was a Battery Algorithm Engineer at Apple Inc., Cupertino, US, where he was in charge of battery management system for Audio products (e.g., AirPods). Dr Song's research interests lie in the areas of modelling, estimation, optimization, and control of energy storage (e.g., battery, supercapacitor, and flywheel) for electrified vehicles and renewable energy systems. Using energy storage as a bridge, his group is actively connecting the automotive, transportation, and power system communities by collaborating on interdisciplinary projects to ensure that both power system and transportation system are efficient, reliable, and clean. Dr. Song is the author or co-author of 2 book chapters and more than 60 peer-reviewed publications including 40 journal articles. He has received several paper awards, including Applied Energy 2015-2016 Highly Cited Paper Award, Applied Energy Award for Most Cited Energy Article from China, NSK Outstanding Paper Award of Mechanical Engineering, and 2013 IEEE VPPC Best Student Paper Award. Dr. Song serves as reviewer for more than 40 international journals. He also serves as Associate Editor for Automotive Innovation, SAE International Journal of Electrified Vehicles and IEEE Transactions on Transportation Electrification.